A critical evaluation of two Reissner–Mindlin type models for composite laminated plates

Wenbin Yu [a], Jun-Sik Kim [b], Dewey H. Hodges [c,*], Maenghyo Cho [d]

[a] *Utah State University, Logan, Utah 80322-4130, USA*
[b] *The Pennsylvania State University, University Park, Pennsylvania 16802, USA*
[c] *Georgia Institute of Technology, Atlanta, Georgia 30332-0150, USA*
[d] *Seoul National University, Seoul, South Korea*

Abstract

The purpose of this paper is to critically evaluate two Reissner–Mindlin type theories developed recently for composite laminated plates, namely, VAPAS (Variational Asymptotic Plate And Shell analysis) and EFSDT (Enhanced First-Order Shear-Deformation Theory). The fundamentals of both models are briefly summarized along with their unique features in comparison to most other existing models. The similarities and differences between VAPAS and EFSDT are also examined. Exact solutions of three-dimensional elasticity theory for the cylindrical bending problems are used as the arbiter to assess the accuracy of both models. Such a systematic assessment demonstrates that both models have achieved an excellent compromise between the layer-wise theories, which are accurate but computationally demanding, and the first-order shear deformation theories, which are computationally cheap but not accurate.
© 2007 Elsevier Masson SAS. All rights reserved.

Keywords: Composite plates; EFSDT; Reissner–Mindlin; Shear deformation theory; Variational asymptotic method; VAPAS

1. Introduction

The use of composite materials in many fields continues to grow. As a result, numerous models for laminated composites can now be found in the literature. Analysis of composite plates with many layers directly using a three-dimensional (3D) formulation is certainly possible but is quite costly and complex. As a result, researchers have strived to reduce the 3D problem to a two-dimensional (2D) one by taking advantage of the small relative size of the plate's thickness compared to other associated length scales. The simplest composite plate theory is classical lamination theory (CLT) based on the Kirchhoff hypothesis, which is commonly understood to be transverse normal remaining rigid and normal during deformation. (Asymptotic derivations of CLT do not require such assumptions.) It is well known, however, that composite plates do not have to be very thick in order for CLT to yield extremely poor results compared to exact 3D solutions. The next logical step beyond CLT is the first-order shear deformation theory (FOSDT). In FOSDT, the transverse normal line, although remaining straight during deformation of the plate, becomes oblique to the deformed surface because of transverse shear. Among all the theories of composite laminates, FOSDT has achieved a reasonable compromise between efficiency and accuracy for global behavior prediction. However, there are at least two deficiencies of FOSDT: 1) the accuracy of FOSDT strongly relies on an accurate estimation of shear correction factors which are difficult to obtain if 3D solutions are not available [11]; 2) FOSDT patently violates the continuity of transverse stress components through the thickness. One cannot expect FOSDT to provide an accurate prediction for the through-the-thickness distribution of stresses and strains, although such information is critical for detailed design and analysis of composite laminates.

Generally speaking, three types of plate theories have been developed to improve upon FOSDT. The first type is referred

---

* Corresponding author.
 E-mail addresses: wenbin.yu@usu.edu (W. Yu), DHodges@GaTech.edu (D.H. Hodges).
 URL: http://www.mae.usu.edu/faculty/wenbin (W. Yu).

to as a higher-order, single-layer theory [13,15]. The basic idea is to use higher-order polynomials or other rational functions to represent the warping of the transverse normal line. The second type is referred to as a zig-zag theory [4–7]. In these theories, piecewise continuous functions along with unit step functions are used for each layer, and then the inter-layer continuity conditions are used to relate different layers. The third type is called a layerwise theory [3,14]. These theories apply the assumptions to each layer and each layer has its own 2D variables. All these theories have better accuracy than FOSDT at the sacrifice of efficiency, among which layerwise theories have the best accuracy yet worst efficiency. Furthermore, some of these theories introduce 2D variables without clear physical meanings.

Very recently, two unique models, namely the variational asymptotic plate and shell analysis (VAPAS) and the enhanced first-order shear deformation theory (EFSDT), have been developed, representing a radical departure from the above approaches. VAPAS is developed by Yu and co-workers [16–19], while EFSDT is developed by Kim and Cho [9,10]. Both models adopt a 2D strain energy form identical to that of FOSDT, but without adopting the assumptions of FOSDT. Below we will refer such models as generalized Reissner–Mindlin theories to distinguish them from FOSDT. Thus, both models maintain the efficiency of FOSDT in the global plate analysis, circumvent the use of shear correction factors, and greatly improved the accuracy of the predicted 3D displacement/stress/strain distributions through the thickness. This paper serves the purpose to critically evaluate both models against each other with the exact 3D solutions as the arbiter, to demonstrate the possibility to use both models as alternatives to expensive 3D finite element analysis if both efficiency and accuracy are equally weighted for design and analysis of composite laminated plates. To this end, we will first introduce the basic concepts of both models, assess the accuracy of both models by comparing them with 3D anisotropic elasticity, and finally point out the advantages and disadvantages of both models.

2. Fundamentals of VAPAS

Mathematically, the approximation in the process of constructing a plate theory stems from elimination of the thickness coordinate as an independent variable of the governing equations, a dimensional reduction process. This sort of approximation is inevitable if one wants to take advantage of the relative smallness of the thickness to simplify the analysis. However, other approximations that are not absolutely necessary should be avoided, if at all possible. For example, for small-strain analysis of plates, it is reasonable to assume that the thickness, h, is small compared to the wavelength of deformation of the reference plane, l. However, it is unnecessary to assume *a priori* some displacement field, although that is the way most plate theories are constructed. As pointed out by [2], the attraction of *a priori* hypotheses is caused by our inability to extract the necessary information from the 3D energy expression.

According to this line of logic, Yu and his co-workers adopted the variational asymptotic method (VAM) introduced by [1], to develop a new approach to modeling composite

laminates [16–19]. These models are implemented in a computer program named VAPAS. In this approach, the original 3D anisotropic elasticity problem is first cast in an intrinsic form, so that the theory can accommodate arbitrarily large displacement and global rotation subject only to the strain being small. An energy functional can be constructed for this nonlinear 3D problem in terms of 2D generalized strain measures and warping functions describing the deformation of the transverse normal:

$$\Pi = \Pi(\epsilon_{11}, \epsilon_{12}, \epsilon_{22}, \kappa_{11}, \kappa_{12}, \kappa_{22}, w_1, w_2, w_3). \tag{1}$$

Here $\epsilon_{11}, \epsilon_{12}, \epsilon_{22}, \kappa_{11}, \kappa_{12}, \kappa_{22}$ are the so-called 2D generalized strains [8] and w_1, w_2, w_3 are unknown 3D warping functions, which characterize the difference between the deformation represented by the 2D variables and the actual 3D deformation for every material point within the plate. It is emphasized here that the warping functions are not assumed *a priori* but are unknown 3D functions to be solved using VAM. Then we can employ VAM to asymptotically expand the 3D energy functional into a series of 2D functionals in terms of the small parameter h/l, such that

$$\Pi = \Pi_0 + \Pi_1 \frac{h}{l} + \Pi_2 \frac{h^2}{l^2} + o\left(\frac{h^2}{l^2}\right), \tag{2}$$

where Π_0, Π_1, Π_2 are governing functionals for different orders of approximation and are functions of 2D generalized strains and unknown warping functions. The unknown warping functions for each approximation can be obtained in terms of 2D generalized strains corresponding to the stationary points of the functionals, which are one-dimensional (1D) analyses through the thickness. Solutions for the warping functions can be obtained analytically as shown in [18] and [16]. After solving for the unknown warping functions, one can substitute them back into the energy functionals in Eq. (1) to obtain 2D energy functionals for 2D plate analysis. For example, for the zeroth-order approximation, the 2D plate model of VAPAS is of the form

$$\Pi_0 = \Pi_0(\epsilon_{11}, \epsilon_{12}, \epsilon_{22}, \kappa_{11}, \kappa_{12}, \kappa_{22}). \tag{3}$$

It should be noted that the energy functional for the zeroth-order approximation, Π_0, coincides to that of CLT; but it is obtained without invoking the Kirchhoff hypothesis and, unlike the classical treatment, the transverse normal is flexible during deformation.

Higher-order approximations can be used to construct refined models. For example, the approximation through second order (h^2/l^2) should be used to handle transverse shear effects. However, there are two challenging issues associated with the second-order approximation:

- The energy functional asymptotically correct up through the second order is in terms of the CLT generalized strains *and their partial derivatives*. This form is not convenient for plate analysis because the boundary conditions cannot be readily associated with quantities normally specified on the boundary of plates.
- Only part of the second-order energy corresponds to transverse shear deformation, and no physical interpretation is known for the remaining terms.

VAPAS uses exact kinematical relations between derivatives of the generalized strains of CLT and the transverse shear strains along with equilibrium equations to meet these challenges. Minimization techniques are then applied to find the transverse shear energy that is closest to the asymptotically correct second-order energy. In other words, the loss of accuracy between the asymptotically correct model and a generalized Reissner–Mindlin model is minimized mathematically. For the purpose of establishing a direct connection between 2D Reissner–Mindlin plate finite element analysis, the through-thickness analysis is implemented using a 1D finite element discretization in the computer program VAPAS, which can be conveniently used by application-oriented engineers.

Compared to most existing composite plate modeling approaches, VAPAS has several unique features:

- VAPAS adopts VAM to rigorously split the original geometrically-exact, nonlinear 3D problem into a linear, 1D, through-the-thickness analysis and a geometrically-exact, nonlinear, 2D, plate analysis. This novel feature allows the global plate analysis to be formulated exactly and intrinsically as a generalized 2D continuum over the reference plane and routes all the approximations into the through-the-thickness analysis, the accuracy of which is guaranteed to be the best by use of the VAM. The optimization procedure minimizes the loss of information in recasting the model to the generalized Reissner–Mindlin form.
- No kinematical assumptions are invoked in the derivation. All deformation of the normal line element is correctly described by the warping functions within the accuracy of the asymptotic approximation.
- VAPAS does not rely on integration of the 3D equilibrium equations through the thickness to obtain accurate distributions of transverse normal and shear strains and stresses.
- VAPAS exactly satisfies all continuity conditions, including those on both displacement and stress, at the interfaces as well as traction conditions on the top and bottom surfaces.

It is important to note that the warping displacements implied by the *a priori* kinematical assumptions of CLT and FOSDT are not equal to the asymptotically exact warping displacements obtained by VAPAS. Those assumed displacements then, contrary to popular opinion, are most certainly *not* asymptotically exact, which is why such theories cannot deliver the accuracy of VAPAS.

3. Fundamentals of EFSDT

Although FOSDT is attractive due to its simplicity, efficiency, and convenience in its treatment of boundary conditions, conventional FOSDT, even aided with appropriate shear correction factors, cannot accurately provide the through-the-thickness variations of displacement, strain, and stress. Generally speaking, there are three challenges to resolve: (a) how to obtain the shear correction factors, (b) how to recover 3D displacement, strain, and stress fields, and (c) how to modify the

kinematic assumptions imposed in conventional FOSDT. Very recently, [9,10] developed an enhanced first-order shear deformation theory (EFSDT) through the reconstruction of an energy in the form of FOSDT using the displacement field obtained from a zig-zag theory [4,5] and a least-square approximation to redefine the displacement variables for FOSDT. Although EFSDT is not founded on such a solid mathematical foundation as VAPAS, various examples have demonstrated its superiority in comparison to conventional FOSDT and higher-order theories. The general form of 3D displacements can be expressed as:

$$
\begin{aligned}
u_\alpha(x_i) &= u_\alpha^o(x_\alpha) - x_3 u_{3,\alpha}^o(x_\alpha) + W_\alpha(x_i), \\
u_3(x_i) &= u_3^o(x_\alpha) + W_3(x_i),
\end{aligned}
\tag{4}
$$

and those of FOSDT are given by

$$
\begin{aligned}
\bar{u}_\alpha(x_i) &= \bar{u}_\alpha^o(x_\alpha) + x_3 \theta_\alpha(x_\alpha), \\
\bar{u}_3(x_i) &= \bar{u}_3^o(x_\alpha),
\end{aligned}
\tag{5}
$$

where the superscript $()^o$ represents the variable at the reference plane, the over-bar $\bar{(\ )}$ indicates the mean value, and W_i represents the 3D through-the-thickness warping functions.

The relaxed definition of the mean displacements can be obtained using the least-square approximation in the average sense. That is,

$$
\left\langle \min_{\bar{u}_i^o, \theta_\alpha} \| u_i - \bar{u}_i \|_2^2 \right\rangle = 0,
\tag{6}
$$

which yields the following relations:

$$
\bar{u}_i^o = u_i^o + \frac{1}{h} \langle W_i \rangle,
\tag{7}
$$

$$
\bar{\gamma}_{\alpha 3} \equiv \theta_\alpha + \bar{u}_{3,\alpha}^o = \frac{12}{h^3} \langle x_3 W_\alpha \rangle.
\tag{8}
$$

Eq. (7) can be further reduced with the kinematic constraint for the transverse normal warping function

$$
\langle W_3 \rangle = 0.
\tag{9}
$$

A 3D strain energy based on 3D variables (u_i^o, W_i) can be written in the compact form of

$$
U^{3D} = U^{3D}(u_i^o, W_i) \approx U(u_i^o, W_\alpha; \sigma_{33} = 0).
\tag{10}
$$

In order to simplify the problem, in-plane warping functions W_α can be split into the through-the-thickness function and the 2D variables as:

$$
W_\alpha(x_i) = \Phi_{\alpha\gamma}(x_3)\, \phi_\gamma(x_\alpha).
\tag{11}
$$

With the aid of Eq. (11), a strain energy, assuming negligible transverse normal stress, given in Eq. (10) can be transformed into a Reissner–Mindlin type strain energy (U_{RM}) using relationships of Eqs. (7) and (8) and the assumed kinematic constraint of Eq. (9) as:

$$
U = U_{RM}(\bar{u}_i^o, \theta_\alpha; \Gamma_{\alpha\gamma}) + U_{TR}(\bar{u}_i^o, \theta_\alpha, \phi_\alpha; C_{\alpha\gamma}, \Gamma_{\alpha\gamma}),
\tag{12}
$$

where a subscript TR represents the truncated strain energy, and

$$
C_{\alpha\gamma} \equiv \langle \Phi_{\alpha\gamma} \rangle, \qquad \Gamma_{\alpha\gamma} \equiv \langle x_3 \Phi_{\alpha\gamma} \rangle,
\tag{13}
$$

which can be determined by minimizing U_{TR} with respect to $C_{\alpha\gamma}$ and $\Gamma_{\alpha\gamma}$ for any strain fields based on $\bar{u}_\alpha^o$, θ_α and ϕ_α.

After solving the problem with a 2D strain energy U_{RM}, one can recover the displacement fields by substituting Eq. (7) into Eq. (4) as:

$$u_\alpha = \bar{u}_\alpha^o - x_3 \bar{u}_{3,\alpha}^o + \left\{ \Phi_{\alpha\gamma}(x_3) - \frac{1}{h} C_{\alpha\gamma} \right\} \Gamma_{\gamma\mu}^{-1} \bar{\gamma}_{\mu 3},$$
$$u_3 = \bar{u}_3^o + W_3,$$
(14)

where $\Phi_{\alpha\gamma}$ is obtained by modifying an EHOPT [4,5], and the out-of-plane warping function W_3 is calculated from the assumption of a negligible transverse normal stress, $\sigma_{33} = 0$, if needed.

After solving for U_{RM}, one can recover the displacements of higher-order theories using relationships that are derived in the least-square approximation, as presented in Eq. (14). Consequently, the stresses are predicted based on the recovered displacements. In-plane stresses are calculated via the constitutive equation, whereas transverse normal and shear stresses can be estimated by using either the constitutive approach or the 3D equilibrium approach.

The current EFSDT formulation is limited to linear elastic problems. Although it is not straightforward to extend it to general nonlinear problems, it is possible to include the von-Kármán partial nonlinearity in EFSDT. In comparison to other composite plate theories based on the FOSDT, the EFSDT has the following features:

- Based on a relaxed definition of mean displacements of the plate, a 3D strain energy is systematically transformed into a 2D strain energy to accurately take transverse shear deformation into account.
- Displacement and stress are recovered by using the same relationships used in the strain energy transformation. This leads to a consistent and systematic one-step recovering procedure.
- Although EFSDT uses 3D equilibrium equations to obtain transverse stresses, it yields good results with the order of derivatives with respect to x_α up to the third order. For example, the second-order and third-order derivatives are needed for transverse normal and shear stresses, respectively.
- EFSDT exactly satisfies continuity conditions on displacement and stress at the interfaces. It exactly satisfies the shear traction conditions on the top and bottom surfaces, whereas it only approximately satisfies the normal traction boundary conditions.

4. Benchmark problems and discussions

To examine and compare the accuracy of VAPAS and EFSDT, we use both to analyze the cylindrical bending problems for two types of plates, laminated and sandwich. For the purpose of comparing with available 3D solutions [12], we here only carry out linear static analyses and focus on the accuracy of stress predictions from both codes. Based on geometry and material information for the plates, we will use VAPAS and EFSDT to obtain the 2D constitutive models for a generalized Reissner–Mindlin plate analysis. The plate analysis for
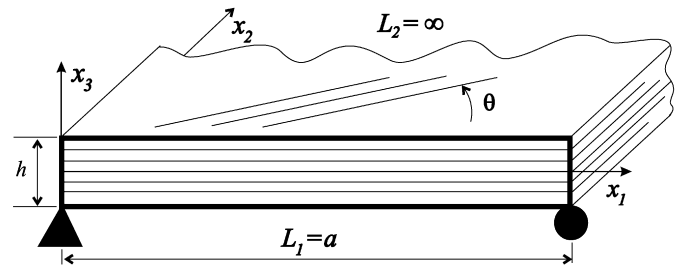

Fig. 1. Cylindrical bending of a composite plate.

this problem can be solved analytically and will provide the required 2D information to feed back into VAPAS and EFSDT to obtain the 3D distributions through the thickness for displacement, strain, and stress.

Fig. 1 sketches the geometry of the plate under consideration. Both plates have layers with material properties given by

$$E_L = 25 \times 10^6 \text{ psi } E_T = 1 \times 10^6 \text{ psi,}$$
$$G_{LT} = 0.5 \times 10^6 \text{ psi } G_{TT} = 0.2 \times 10^6 \text{ psi,}$$
$$\nu_{LT} = \nu_{TT} = 0.25,$$
(15)

where L denotes the fiber direction and T denotes a direction perpendicular to the fiber. For the sandwich plate, the material properties of the face sheets are given in Eq. (15), and the core is assumed to be isotropic with $E = 0.145 \times 10^5$ and $\nu = 0.25$. This assumption is only made for simplicity; both VAPAS and EFSDT can handle a core made of anisotropic material.

As shown in Fig. 1, the plate has width a along the x_1 direction, infinite length along the x_2 direction, and thickness h in the x_3 direction. Two width to thickness ratios are used: $a/h = 4$ for the laminated plates, and $a/h = 10$ for the sandwich plate. The plates are both taken to be simply supported and subjected to a sinusoidal surface loading of the form

$$p\left(x_1, \pm \frac{h}{2}\right) = \pm \frac{p_0}{2} \sin\left(\frac{\pi x_1}{a}\right).$$
(16)

The following five cases with different symmetry and layups are investigated:

- case 1: antisymmetric angle ply, $[15°/-15°]$;
- case 2: symmetric angle ply, $[30°/-30°/-30°/30°]$;
- case 3: symmetric nearly cross ply, $[0.5°/90.5°/90.5°/0.5°]$;
- case 4: 20 layers with symmetric layup as $[30°/-30°/-30°/30°]_5$;
- case 5: sandwich plate with symmetric layup as $[0.05°/\text{Core}(0.05°)/0.05°]$, where the thickness of each face sheet is equal to $h/10$.

We change slightly the ply angle from cross ply in case 3 to allow us to use a single analytical solver for angle ply layups to obtain exact solutions. For the same reason, we made the core material slightly different from isotropy ($E_2 = E_3 = 1.00001E$) first then assign a tiny ply angle to make it an angle ply.

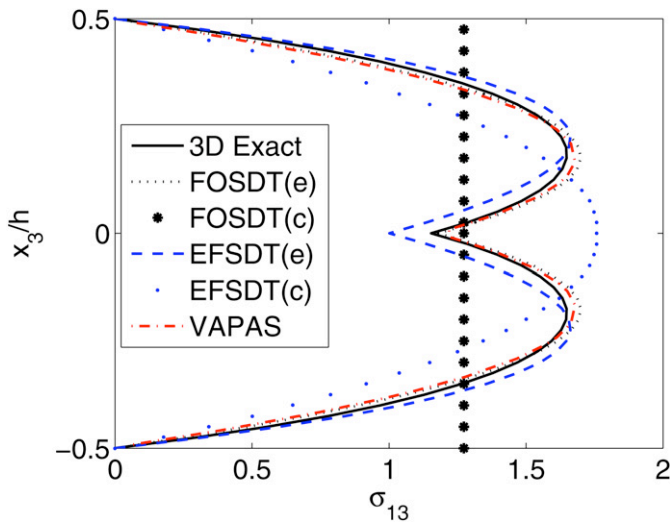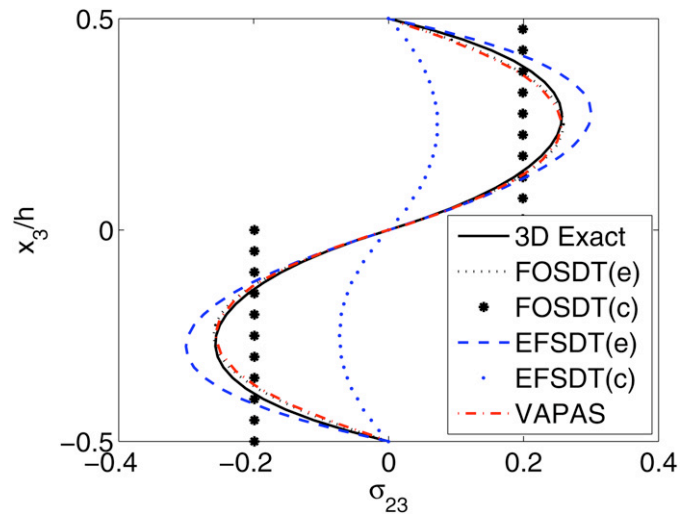Fig. 2. Through-the-thickness variation of σ_{13} (case 1).

Fig. 3. Through-the-thickness variation of σ_{23} (case 1).

4.1. Through-the-thickness variations of stresses

To present the results graphically, we normalize the stresses by the transverse pressure p_0 such that $\bar{\sigma}_{ij} = \frac{\sigma_{ij}}{p_0}$. In all the plots shown below, solid lines represent the 3D exact solutions [12], and dash-dotted lines denote VAPAS solutions, which are obtained directly by using the recovery relations provided by the model itself. In contrast to VAPAS, for EFSDT there are two types of recovered 3D transverse shear and normal stresses (σ_{i3}): 1) EFSDT(e), obtained by integrating the derivatives of recovered in-plane stresses using the 3D equilibrium equations, denoted by dashed lines in the plots; and 2) EFSDT(c), obtained using the constitutive relations based on 3D strains, denoted by small dots in the plots. To show the advantages of VAPAS and EFSDT compared to conventional FOSDT, results from FOSDT with the shear correction factor of 5/6 are also plotted in some of the figures. Similar to EFSDT, FOSDT(e) is obtained using 3D equilibrium equations and denoted by dotted lines, and FOSDT(c) is obtained directly using constitutive relations and denoted by bullets. For the sake of saving space, we mainly plot transverse stress components (σ_{i3}); most of existing theories cannot provide an accurate yet efficient prediction for these components. We also show some in-plane stress components where large discrepancies are exhibited among the different approaches. In all the figures, stresses are calculated at points where their maximum values occur ($\sigma_{\alpha\beta}$ and σ_{33} at $x_1 = a/2$, and $\sigma_{\alpha 3}$ at $x_1 = 0, a$).

First, laminated composite plates with 2 angle-ply layers (case 1) are investigated. The 3D stress distributions through the thickness as predicted by the different approaches are plotted in Figs. 2–4. From these plots, one can observe that VAPAS achieves the best accuracy for all the transverse components for this case. FOSDT(e) provides a pretty good prediction for transverse shear stresses, whereas EFSDT(e) shows a worse prediction than FOSDT(e) for these two stress components. Both EFSDT(e) and FOSDT(e) predict the transverse normal stress reasonably well. However, EFSDT(e) does not satisfy the boundary conditions. Although FOSDT(e) satisfies the bound-
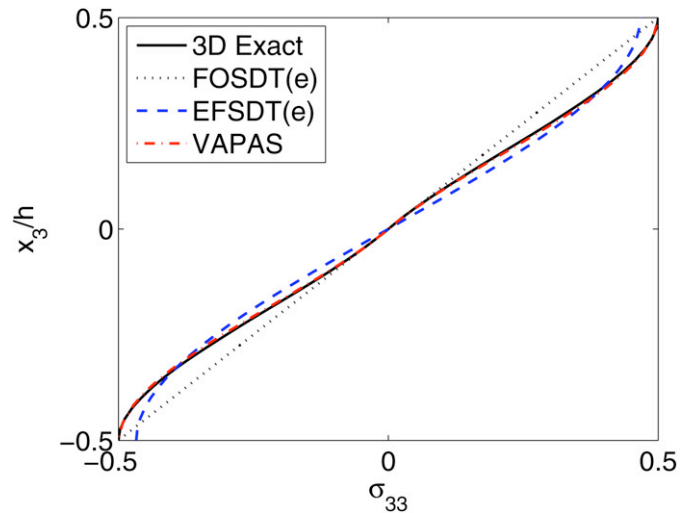

Fig. 4. Through-the-thickness variation of σ_{33} (case 1).

ary conditions, its prediction is even worse than EFSDT(e). Neither EFSDT(c) nor FOSDT(c) is predictive at all for the transverse shear stresses, and transverse normal stresses are not even available from these two approaches.

For case 2, the transverse stress components are plotted in Figs. 5–7. As one can see from Fig. 5, EFSDT(e) best captures the shape of the stress curve, especially the kinking behavior at the interface of laminae. However, the quantitative agreement of EFSDT(e) results is slightly worse than those of VAPAS, FOSDT(e), and EFSDT(c). For σ_{23}, shown in Fig. 6, again, EFSDT captures the shape very well. However, quantitatively, VAPAS achieves the best accuracy among all the approaches. As shown in Fig. 7, VAPAS is almost on the top of exact solutions, and EFSDT(e) has pretty good agreement with a slight discrepancy at the boundaries.

For case 3, we find out that there are huge differences among the different approaches for the in-plane stress σ_{22} as shown in Fig. 8. It is seen that VAPAS is far better than both EFSDT and FOSDT. It is noted that in-plane components of EFSDT and FOSDT are calculated directly using the plane-stress re-
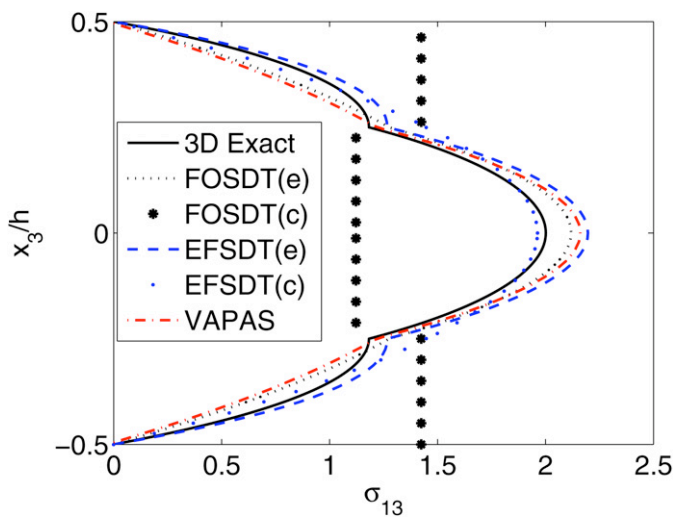
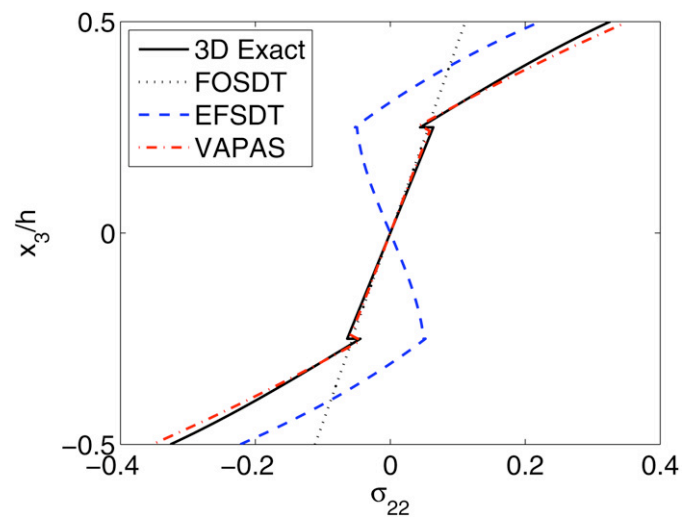Fig. 5. Through-the-thickness variation of σ_{13} (case 2).

Fig. 8. Through-the-thickness variation of σ_{22} (case 3).
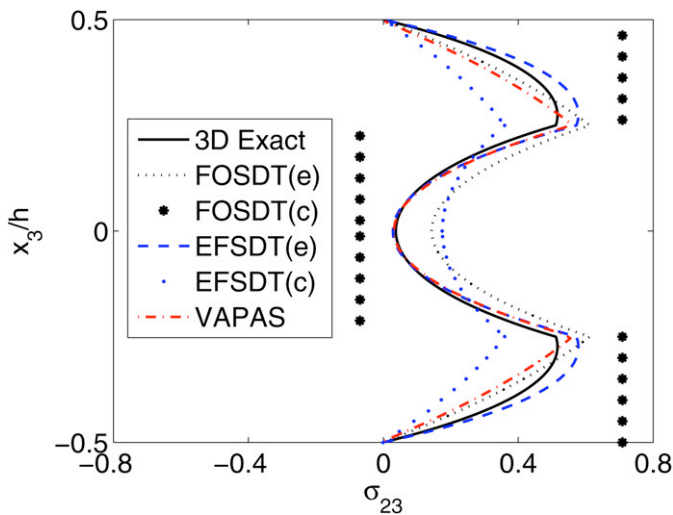

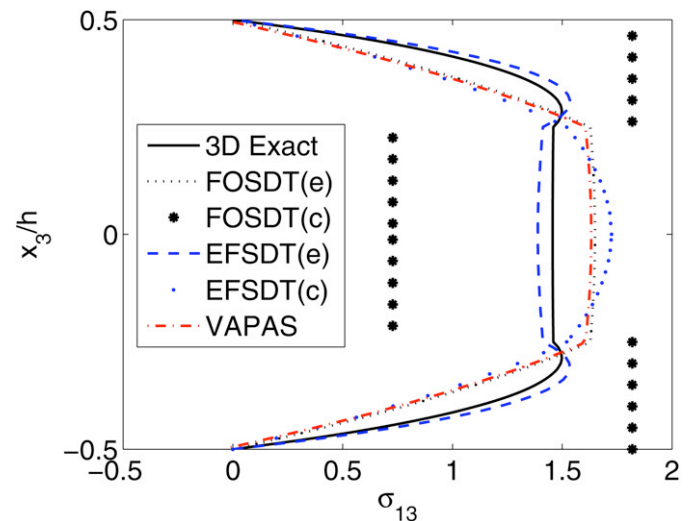Fig. 6. Through-the-thickness variation of σ_{23} (case 2).

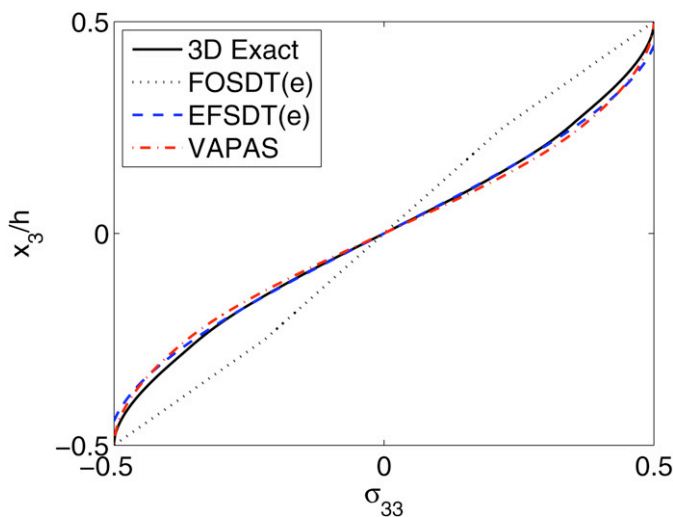Fig. 9. Through-the-thickness variation of σ_{13} (case 3).

Fig. 7. Through-the-thickness variation of σ_{33} (case 2).

duced material properties. This can be explained by noting that σ_{22} is dominated by Poisson's effects induced from σ_{11} and σ_{33} in the cylindrical bending problem. For this particular lay-up $[0.5°/90.5°/90.5°/0.5°]$, σ_{33} plays an important role in predicting σ_{22}, which implies that it could be essential to use 3D constitutive equations for certain cases. In other words, theories with unjustified kinematical assumptions might fail for certain cases. The transverse shear stress σ_{13} is plotted in Fig. 9, where EFSDT(e) shows excellent agreement with the exact solution for σ_{13}, while VAPAS yields similar results to FOSDT(e) and EFSDT(c). (We do not need to plot for σ_{23} because it has a similar trend for different approaches with much smaller magnitude.) From Fig. 10, one can see that both VAPAS and EFSDT(e) produce much better results than FOSDT(e) for the transverse normal stress, with only VAPAS satisfying the boundary conditions.

In order to examine more practical layups, we study a composite plate with 20 layers and a symmetric angle-ply layup (case 4). The transverse shear stresses are plotted in Figs. 11
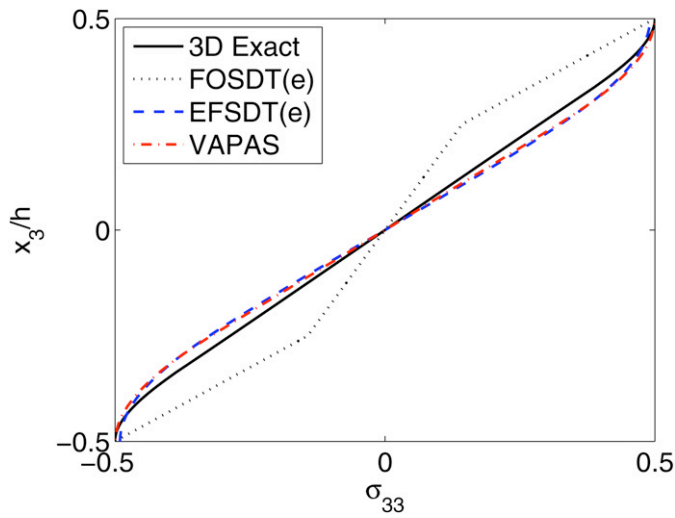
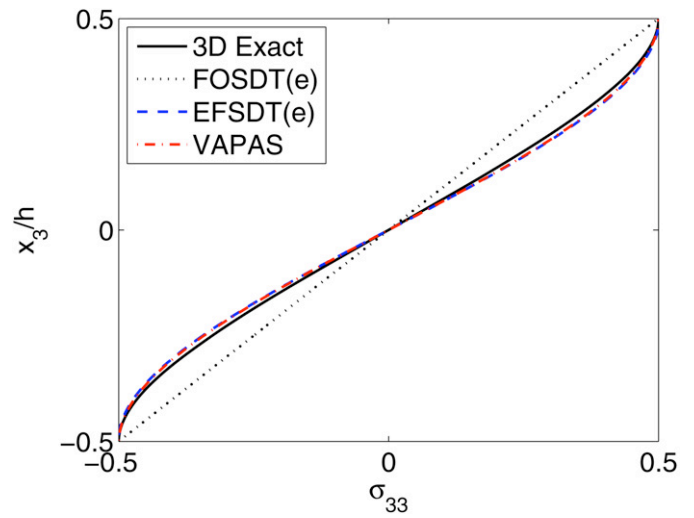Fig. 10. Through-the-thickness variation of σ_{33} (case 3).

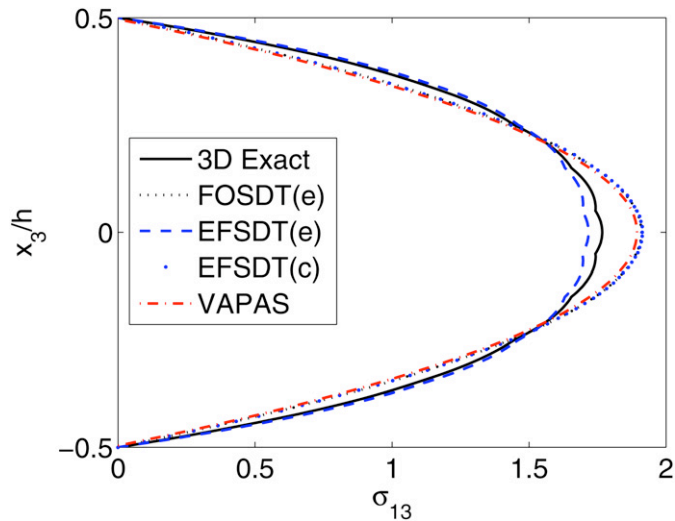Fig. 13. Through-the-thickness variation of σ_{33} (case 4).

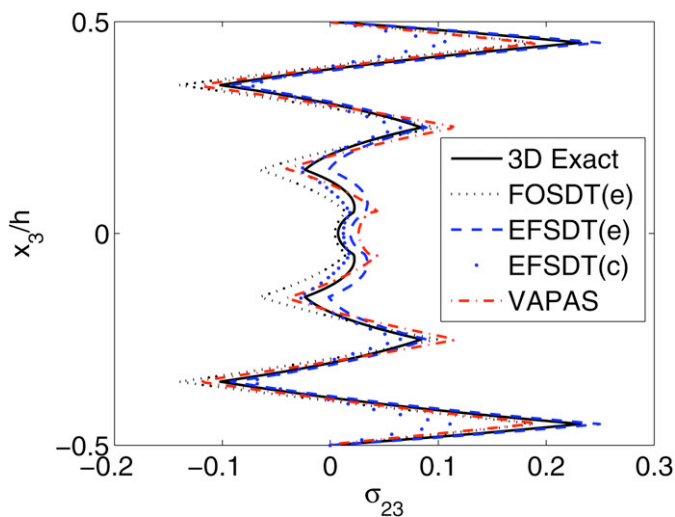Fig. 11. Through-the-thickness variation of σ_{13} (case 4).

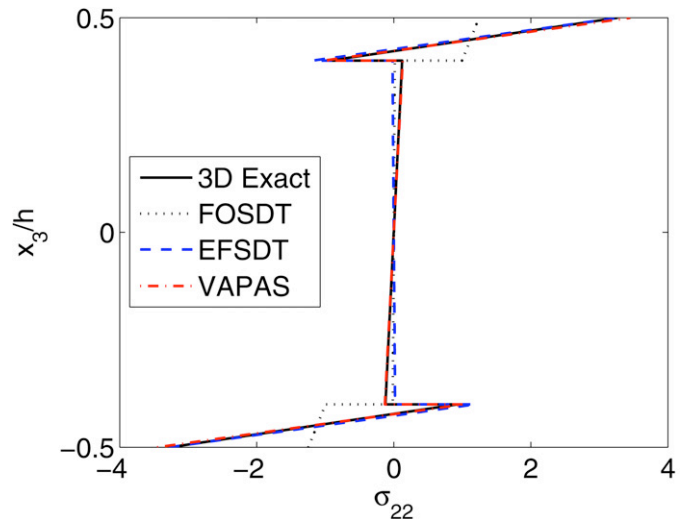Fig. 14. Through-the-thickness variation of σ_{22} (case 5).

Fig. 12. Through-the-thickness variation of σ_{23} (case 4).

and 12. It is observed that there are two groups showing similar results for σ_{13} shown in Fig. 11. One is EFSDT(e) and the other is EFSDT(c), FOSDT(e) and VAPAS. For σ_{23} presented in Fig. 12, EFSDT(e) can accurately predict the qualitative behavior near the mid-plane, whereas the prediction at the interfaces is deteriorated. It is seen that the accuracy of EFSDT increases as the number of layers increases compared to VAPAS. FOSDT(c) results are not shown because they are too off from the exact solutions. For the transverse normal stress presented in Fig. 13, both EFSDT(e) and VAPAS show excellent agreement with the exact solution.

Lastly, a sandwich plate with $a/h = 10$ (case 5) is considered to investigate the significant shear deformation effect due to the core material. Fig. 14 shows the through-the-thickness variation of σ_{22}. Both VAPAS and EFSDT(e) capture very well the sudden change at the interface, with VAPAS doing much better than EFSDT(e). The reason is similar to what we pointed out for case 3: The transverse normal effect due to a particular lay-up of [0.05°/Core(0.05°)/0.05°] will affect the prediction
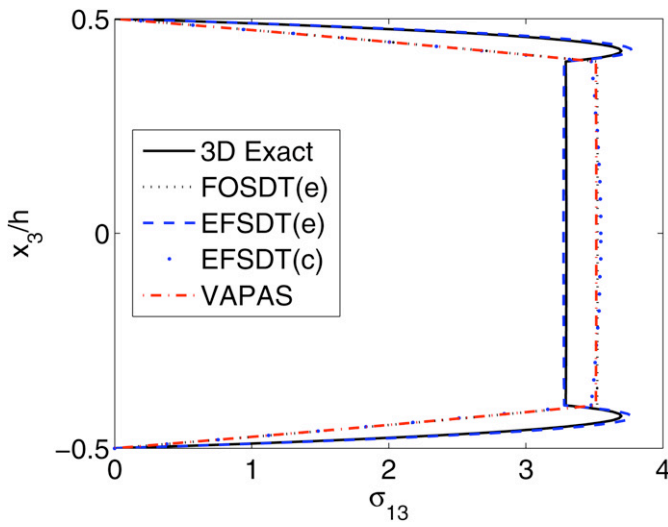
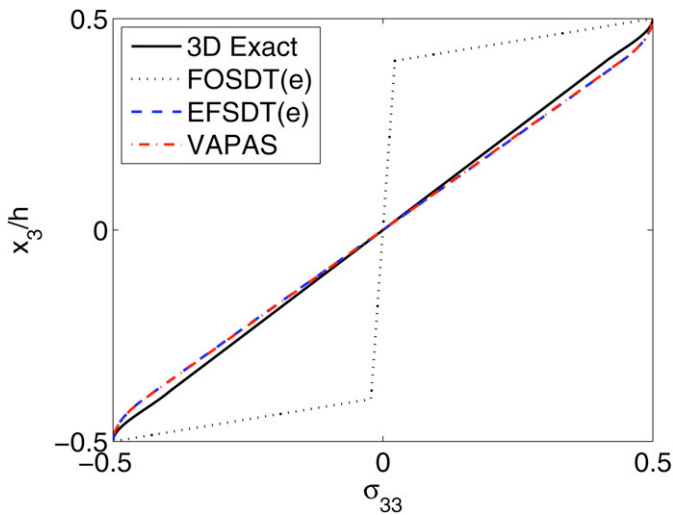Fig. 15. Through-the-thickness variation of σ_{13} (case 5).

Fig. 16. Through-the-thickness variation of σ_{33} (case 5).

Table 1
Comparison of stress metrics for case 1

Stresses	3D	FOSDT		VAPAS		EFSDT	
	M_{ij}	M_{ij}	(E_{ij})	M_{ij}	(E_{ij})	M_{ij}	(E_{ij})
σ_{11} ($x_3 = 0.50h$)	16.324	13.449	(11.2)	17.756	(9.39)	17.466	(15.6)
σ_{22} ($x_3 = 0.50h$)	1.3697	1.0267	(13.2)	1.4802	(8.53)	1.3477	(19.9)
σ_{12} ($x_3 = 0.50h$)	3.3676	2.6419	(11.6)	3.6846	(9.11)	3.8213	(17.3)
σ_{13} ($x_3 = 0.00h$)	1.1534	1.1791	(3.41)	1.1701	(3.59)	1.0012	(5.64)
σ_{23} ($x_3 = 0.25h$)	0.2556	0.2594	(5.02)	0.2561	(5.71)	0.2971	(14.3)
σ_{33} ($x_3 = 0.50h$)	0.5000	0.5000	(12.1)	0.4994	(1.19)	0.4667	(7.16)

Table 2
Comparison of stress metrics for case 2

Stresses	3D	FOSDT		VAPAS		EFSDT	
	M_{ij}	M_{ij}	(E_{ij})	M_{ij}	(E_{ij})	M_{ij}	(E_{ij})
σ_{11} ($x_3 = 0.50h$)	13.413	8.6636	(24.6)	14.296	(4.59)	14.598	(10.2)
σ_{22} ($x_3 = 0.50h$)	4.2395	2.6653	(28.0)	4.5160	(4.54)	4.5467	(8.60)
σ_{12} ($x_3 = 0.50h$)	6.4854	4.1561	(24.5)	6.9304	(5.00)	7.2489	(13.4)
σ_{13} ($x_3 = 0.00h$)	2.0009	2.1186	(8.02)	2.1612	(9.82)	2.1962	(8.63)
σ_{23} ($x_3 = 0.25h$)	0.5116	0.6120	(28.9)	0.5586	(15.5)	0.5728	(12.1)
σ_{33} ($x_3 = 0.50h$)	0.5000	0.5000	(24.6)	0.5000	(4.07)	0.5097	(2.69)

Table 3
Comparison of stress metrics for case 3

Stresses	3D	FOSDT		VAPAS		EFSDT	
	M_{ij}	M_{ij}	(E_{ij})	M_{ij}	(E_{ij})	M_{ij}	(E_{ij})
σ_{11} ($x_3 = 0.50h$)	19.935	11.053	(55.1)	22.607	(15.9)	22.060	(18.2)
σ_{22} ($x_3 = 0.50h$)	0.3258	0.1113	(58.5)	0.3527	(6.39)	0.2222	(79.3)
σ_{12} ($x_3 = 0.50h$)	0.1572	0.0852	(47.2)	0.1790	(16.7)	0.1753	(18.3)
σ_{13} ($x_3 = 0.25h$)	1.4599	1.6277	(15.2)	1.6051	(15.6)	1.4123	(4.91)
σ_{23} ($x_3 = 0.25h$)	0.0107	0.0125	(19.4)	0.0119	(16.7)	0.0103	(5.15)
σ_{33} ($x_3 = 0.50h$)	0.5000	0.5000	(29.7)	0.5000	(6.91)	0.4909	(7.59)

from EFSDT(e) for in-plane components. VAPAS can accurately capture such effects because there are no *a priori* kinematical assumptions involved in the theory, and 3D effects are taken into account. The transverse shear stress σ_{13} is presented in Fig. 15. The result of FOSDT(c) is omitted, since it is too far away from the exact solution. Even if the sandwich plate is moderately thick, FOSDT(e), EFSDT(c) and VAPAS does not capture the kinky shape in the vicinity of the interface whereas EFSDT(e) does. (The plot for σ_{23} is skipped because the different approaches exhibit a similar trend with much smaller magnitude.) Fig. 16 shows the transverse normal stress distribution. One can see that σ_{33} by FOSDT(e) is very poor near the core portion, and both VAPAS and EFSDT(e) have excellent agreement with the exact solution.

4.2. Comparison of quantitative behaviors

From all the plots, we can conclude that both EFSDT(e) and VAPAS provide comparable, excellent agreement with the exact solutions. However, to assess the stress prediction more quantitatively, we must define a metric and examine the results in its light. We calculate the maximum stresses occurring either at the interface or at the top surface, which are defined as M_{ij}^{Theory}. This metric will be used to measure the magnitude of stress components predicted by different theories including 3D, FOSDT, VAPAS and EFSDT. Notice here that all the transverse stresses from FOSDT and EFSDT are obtained by the equilibrium approach in this section.

To measure the loss of accuracy caused by approximations in FOSDT, VAPAS and EFSDT, we define another metric to measure the relative difference between both models and 3D solutions as:

$$E_{ij} = \frac{\int_{-h/2}^{h/2} |\sigma_{ij}^{\text{3D}} - \sigma_{ij}^{\text{Approx.}}| \, dx_3}{\int_{-h/2}^{h/2} |\sigma_{ij}^{\text{3D}}| \, dx_3} \times 100 \tag{17}$$

where $\sigma_{ij}^{\text{Approx.}}$ will be replaced with the stress components predicted by FOSDT, VAPAS and EFSDT to calculate E_{ij} for corresponding models.

In Tables 1–5, results using the two metrics M_{ij} and E_{ij} are listed and compared. For all the cases investigated here, the relative difference of in-plane stresses predicted by VAPAS and 3D results is noticeably smaller than those by EFSDT for cases

Table 4
Comparison of stress metrics for case 4

Stresses	3D	FOSDT		VAPAS		EFSDT	
	M_{ij}	M_{ij}	(E_{ij})	M_{ij}	(E_{ij})	M_{ij}	(E_{ij})
σ_{11} ($x_3 = 0.50h$)	12.917	9.6025	(22.9)	13.741	(6.43)	13.644	(6.67)
σ_{22} ($x_3 = 0.50h$)	4.1976	3.0616	(24.2)	4.4619	(6.17)	4.3490	(8.04)
σ_{12} ($x_3 = 0.50h$)	6.7360	5.0803	(21.3)	7.1790	(6.66)	7.2136	(6.62)
σ_{13} ($x_3 = 0.00h$)	1.7672	1.9101	(6.76)	1.8942	(7.11)	1.7170	(2.13)
σ_{23} ($x_3 = 0.45h$)	0.2320	0.1895	(44.0)	0.1855	(33.3)	0.2496	(24.4)
σ_{33} ($x_3 = 0.50h$)	0.5000	0.5000	(17.4)	0.5000	(2.92)	0.5009	(3.43)

Table 5
Comparison of stress metrics for case 5

Stresses	3D	FOSDT		VAPAS		EFSDT	
	M_{ij}	M_{ij}	(E_{ij})	M_{ij}	(E_{ij})	M_{ij}	(E_{ij})
σ_{11} ($x_3 = 0.50h$)	314.08	124.49	(75.2)	332.65	(5.98)	327.78	(5.67)
σ_{22} ($x_3 = 0.50h$)	3.2661	1.2450	(84.8)	3.4518	(5.81)	3.2780	(24.9)
σ_{12} ($x_3 = 0.50h$)	0.2383	0.1011	(74.3)	0.2522	(6.19)	0.2482	(6.14)
σ_{13} ($x_3 = 0.40h$)	3.2912	3.5200	(11.5)	3.5106	(11.3)	3.2799	(0.87)
σ_{23} ($x_3 = 0.40h$)	0.0020	0.0029	(38.9)	0.0022	(13.6)	0.0020	(2.67)
σ_{33} ($x_3 = 0.50h$)	0.5000	0.5000	(76.4)	0.5000	(5.57)	0.4993	(5.78)

1 and 2, whereas VAPAS and EFSDT have similar predictions for cases 3–5 except σ_{22} for cases 3 and 5. Because of their relatively large magnitude, accurate prediction of in-plane stress components is important for analyzing both global plate behavior and local failure analysis of the structures. It is seen that both VAPAS and EFSDT are much better than FOSDT except case 1, especially for case 5 (a sandwich plate) where the relative difference of in-plane stresses predicted by FOSDT is larger than 70%. For this reason, henceforth, discussion will be focused on comparison between VAPAS and EFSDT. For transverse components, we have to carry out this comparison case by case.

As shown in Table 1, the relative difference between VAPAS and 3D predictions for transverse components is much smaller than those of EFSDT for a two-layered angle-ply plate (case 1). For case 2, which is a four-layered plate, one can observe from Table 2 that the relative difference for VAPAS predictions is larger than those of EFSDT. It is interesting to notice that M_{13}^{VAPAS} is closer to the exact solution than M_{13}^{EFSDT}, while E_{13}^{EFSDT} is less than E_{13}^{VAPAS}. This can be deduced from the fact that EFSDT can capture the kinking behavior better than VAPAS; see Fig. 5. The quantitative metrics for cases 3–5 are listed in Tables 3, 4, and 5, respectively. EFSDT provides better predictions for transverse shear stresses, while VAPAS provides better predictions for transverse normal stresses.

We have to admit that the metrics we defined are not perfect ones for one to accurately tell the difference between VAPAS and EFSDT. The metric values should be viewed together with the corresponding plots to provide a better assessment of the theories. It is believed that if an appropriate metric such as the energy stored in the plates can be defined, VAPAS should be closer to the exact solution in comparison to EFSDT because the energy loss between a Reissner–Mindlin model and 3D exact formulation is minimized by VAPAS. Both models, however, show accurate predictions on the metrics used in the present assessment. Thus, they are both of practical use in the analysis of laminated composite and sandwich plates.

Another interesting finding is that recovering the 3D stresses using 3D equilibrium equations plays an important role for obtaining accurate transverse shear stresses. This is believed to be the main reason for the fact that the relative difference metric of EFSDT is smaller than VAPAS for transverse shearing stress components, even though they are obtained from in-plane components that are not as accurate. This further means that if one recovers 3D transverse shear stresses from VAPAS in-plane components, the predictions will be much better that EFSDT. However, the authors of VAPAS chose not to do so for the simple reason that the linear 3D equilibrium equations are not inherent in the their theory, which is nonlinear, and such recovery is therefore not applicable to nonlinear problems.

5. Advantages and disadvantages of VAPAS and EFSDT

The cases we just studied have clearly shown that both VAPAS and EFSDT are capable of providing far better predictions than FOSDT and higher-order theories for 3D stress distributions with the same computational cost for the global plate analysis as FOSDT (i.e. five degrees of freedom per node for plate elements). It has adequately demonstrated that these two models are superior to most existing approaches for achieving an excellent tradeoff between efficiency and accuracy. However, these two approaches are drastically different from each other in many aspects. In this section, we are going to further compare VAPAS and EFSDT to point out advantages and disadvantages of both theories from the view points of their theoretical formulations and their numerical accuracy and efficiency.

5.1. Theoretical formulations

VAPAS adopts VAM to rigorously split the original, nonlinear 3D problem into a 1D through-the-thickness analysis and a 2D nonlinear plate analysis. VAPAS provides a mechanism to formulate the 2D plate analysis intrinsically as a generalized continuum with exact kinematics. The advantage of VAPAS is that no kinematical assumptions are invoked in the formulation and all the deformations of the transverse normal are described by the 3D unknown warping functions that are asymptotically solved by the VAM. The disadvantage is that it involves some advanced mathematics and so may appear arcane to engineers.

EFSDT relaxes the kinematic constraints of conventional FOSDT using piecewise continuous, warping functions from higher-order zig-zag theories, and recasts the 3D strain energy into a Reissner–Mindlin model. The advantage of EFSDT is that better warping functions can always be adopted due to its *ad hoc* nature and its derivation is relatively simpler than VAPAS. The disadvantage is that *ad hoc* assumptions introduce arbitrariness, and thus it may fail for certain cases. Examples, although few, have found in the previous section that EFSDT might be worse than FOSDT. It is, however, believed by the authors of EFSDT that most of them can be resolved

by incorporating the 3D constitutive relations. Finally, the current EFSDT formulation is limited to geometrically nonlinear problems associated with moderate rotations. It would not be straightforward to extend it to nonlinear problems of the geometrically exact variety.

5.2. Numerical accuracy and efficiency

As revealed by the benchmark problems herein and their theoretical formulations, both VAPAS and ESFDT satisfy interface continuity for displacements and stresses. VAPAS also satisfies arbitrary surface traction boundary conditions. On the other hand, EFSDT only satisfies surface traction shear boundary conditions exactly; the normal traction boundary conditions cannot be satisfied by EFSDT. An additional advantage of VAPAS is that 3D constitutive equations are used to calculate all the stresses. Its accuracy is consistent for all the problems we have studied. The advantage of EFSDT is that the 3D stresses, particularly the transverse shear stresses, recovered using 3D equilibrium equations can capture the kinking behavior pretty well. The main disadvantage of VAPAS is that it requires third-order derivatives of plate displacements for accurate prediction of 3D in-plane stresses and transverse normal stresses, which might not be available from lower-order plate elements. The main disadvantage of EFSDT is that it may neglect some important effect such as the transverse normal effect to σ_{22}; see Fig. 8. Without exact solution, such deficiencies are not easy to be detected.

Both VAPAS and EFSDT analyze composite plates using a three-step procedure: 1) obtain a 2D Reissner–Mindlin type constitutive model; 2) carry out the global plate analysis using the obtain constitutive model; 3) recover the 3D distribution through the thickness based on the results from the global analysis. The computing time needed for the first step and the third step is negligible compared to the second step. Hence their efficiency will be similar as far as the complete solution concerned.

6. Conclusions

This paper has assessed two recently developed Reissner–Mindlin type theories for composite laminated plates, VAPAS and EFSDT. The fundamentals of both models are briefly summarized along with their unique features in comparison to most other existing models. The similarities and differences between VAPAS and EFSDT are also examined. It is observed that VAPAS achieves a consistent prediction for all the cases, yet EFSDT can predict better transverse shear stresses for some cases, particularly when the number of layers become larger and the transverse shear deformation is significant. Nevertheless, both methods have achieved an excellent compromise between the layer-wise theories, which are accurate but computationally demanding, and the first-order shear deformation theories, which are computationally cheap but not accurate. They are recommended to use in place of expensive 3D finite element analysis if both efficiency and accuracy are needed to be considered during design and analysis of composite laminates.

References

[1] V.L. Berdichevsky, Variational-asymptotic method of constructing a theory of shells, PMM 43 (4) (1979) 664–687.

[2] V.L. Berdichevsky, Variational-asymptotic method of constructing the nonlinear shell theory, in: Theory of Shells, North-Holland Publishing Company, 1980, pp. 137–161.

[3] E. Carrera, Mixed layer-wise models for multilayered plates analysis, Composite Structures 43 (1998) 57–70.

[4] M. Cho, R.R. Parmerter, An efficient higher order plate theory for laminated composites, Composite Structures 20 (2) (1992) 113–123.

[5] M. Cho, R.R. Parmerter, Efficient higher order composite plate theory for general lamination configurations, AIAA Journal 31 (7) (1993) 1299–1306.

[6] Y.B. Cho, R.C. Averill, First-order zig-zag sublaminate plate theory and finite element model for laminated composite and sandwich panels, Composite Structures 50 (2000) 1–15.

[7] M. DiSciuva, Development of anisotropic multilayered shear deformable rectangular plate element, Computers and Structures 21 (1985) 789–796.

[8] D.H. Hodges, A.R. Atılgan, D.A. Danielson, A geometrically nonlinear theory of elastic plates, Journal of Applied Mechanics 60 (1) (March 1993) 109–116.

[9] J.-S. Kim, M. Cho, Enhanced first-order shear deformation theory for laminated and sandwich plates, Journal of Applied Mechanics 72 (2005) 809–817.

[10] J.-S. Kim, M. Cho, Enhanced modeling of laminated and sandwich plates via strain energy transformation, Composites Science and Technology 66 (11–12) (September 2006) 1575–1587.

[11] A.K. Noor, W.S. Burton, Assessment of shear deformation theories for multilayered composite plates, Applied Mechanics Review 41 (1) (1989) 1–13.

[12] N.J. Pagano, Influence of shear coupling in cylindrical bending of anisotropic laminates, Journal of Composite Materials 4 (July 1970) 330–343.

[13] J.N. Reddy, A simple higher-order theory for laminated composite plates, Journal of Applied Mechanics 51 (1984) 745–752.

[14] D.H. Robbins, J.N. Reddy, Modeling of thick composites using a layerwise laminate theory, International Journal for Numerical Methods in Engineering 36 (1993) 655–677.

[15] M. Touratier, An efficient standard plate theory, International Journal of Engineering Science 29 (1991) 901–916.

[16] W. Yu, Mathematical construction of a Reissner–Mindlin plate theory for composite laminates, International Journal of Solids and Structures 42 (2005) 6680–6699.

[17] W. Yu, D.H. Hodges, An asymptotic approach for thermoelastic analysis of laminated composite plates, Journal of Engineering Mechanics 130 (5) (2004) 531–540.

[18] W. Yu, D.H. Hodges, V.V. Volovoi, Asymptotic construction of Reissner-like models for composite plates with accurate strain recovery, International Journal of Solids and Structures 39 (20) (2002) 5185–5203.

[19] W. Yu, D.H. Hodges, V.V. Volovoi, Asymptotically accurate 3-D recovery from Reissner-like composite plate finite elements, Computers and Structures 81 (7) (2003) 439–454.